



Cite this: *Polym. Chem.*, 2019, **10**, 4665

3D printable non-isocyanate polyurethanes with tunable material properties†

John J. Warner,^a Pengrui Wang,^a William M. Mellor,^a Henry H. Hwang,^a Ji Hoon Park,^b Sang-Hyun Pyo^{id}*^c and Shaochen Chen^{id}*^a

Green chemistry-based non-isocyanate polyurethanes (NIPU) are synthesized and 3D-printed *via* rapid, projection photopolymerization into compliant mechanisms of 3D structure with spatially-localized material properties. Trimethylolpropane allyl ether-cyclic carbonate is used to couple the unique properties of two types of reaction chemistry: (1) primary diamine-cyclic carbonate ring-opening conjugation for supplanting conventional isocyanate-polyol reactions in creating urethane groups, with the additional advantage of enabling modular segment interchangeability within the diurethane prepolymers; and (2) thiol-ene (click) conjugation for non-telechelic, low monodispersity, quasi-crystalline-capable, and alternating step-growth co-photopolymerization. Fourier transform infrared spectroscopy is used to monitor the functional group transformation in reactions, and to confirm these process-associated molecular products. The extent of how these processes utilize molecular tunability to affect material properties were investigated through measurement-based comparison of the various polymer compositions: frequency-related dynamic mechanical analysis, tension-related elastic-deformation mechanical analysis, and material swelling analysis. Stained murine myoblasts cultured on NIPU slabs were evaluated *via* fluorescent microscopy for “green-chemistry” affects on cytocompatibility and cell adhesion to assess potential biofouling resistance. 3D multi-material structures with micro-features were printed, thus demonstrating the capability to spatially pattern different NIPU materials in a controlled manner and build compliant mechanisms.

Received 6th July 2019,
Accepted 16th July 2019

DOI: 10.1039/c9py00999j

rsc.li/polymers

Introduction

Eliminating and replacing the use of hazardous substances remains a major challenge in terms of human health, wildlife, and environmental impact. Therefore, biocompatible and non-toxic materials are playing an increasingly prominent role in the fast-growing fields of biomedical devices, tissue engineering, and regenerative medicine.¹ Recently, the rising popularity of 3D printing for biomedical applications has renewed interest in printable polymers with tunable, biocompatible, and desirable mechanical properties.^{2–4} Current trends in the synthesis of biocompatible photopolymers for light-based 3D

printing rely on the modification of naturally-derived hydrogels, usually due to a desire to recapitulate native microenvironments in the final printed construct. Although naturally originated polymers such as polysaccharides (*e.g.* alginate, chitosan, starch, cellulose, hyaluronan), proteins and their derivatives are frequently employed due to their biocompatibility,⁵ these natural materials have been incorporated into photopolymers *via* the addition of terminal acrylates, or other similar methods.⁶ As an example, in a telechelic polymer with terminal acrylate groups as a crosslinker, polymerized acrylate chains create a synthetic interpenetrating network (IPN). This has been conceptualized like non-parallel “ladder rails” connecting existing natural polymer fragments together as skewed “ladder steps”, at every-other carbon in the “rail” chain. This general method extends photopolymerization capability or control to more materials and largely constrains mainstream acrylate IPNs to single-carbon spacing unless adding plasticizers (*e.g.* isobornyl acrylate, ethyl acrylate). However, plasticizer toxicity unfortunately limits material use and material tunability *via* the IPN for some applications.

As such, many of the conventional hybridized polymer hydrogels used still suffer inadequate strength and durability

^aDepartment of NanoEngineering, University of California, San Diego, 9500 Gilman Drive, La Jolla, CA 92093, USA. E-mail: chen168@eng.ucsd.edu

^bCarbon Resources Institute, Korea Research Institute of Chemical Technology (KRICT), Daejeon, Republic of Korea

^cBiotechnology, Department of Chemistry, Center for Chemistry and Chemical Engineering, Lund University, Box 124, 221 00 Lund, Sweden.

E-mail: sang-hyun.pyo@biotek.lu.se

† Electronic supplementary information (ESI) available. See DOI: 10.1039/c9py00999j

for many current needs. Often these materials do not match well with the physical and mechanical application demands for tissue and organ regeneration.⁷

As a synthetic alternative, in recent years, new polyurethanes (PUs) have been developed and incorporated in a variety of biomedical applications^{7–11} due to their excellent mechanical strength, flexibility, hydrophobicity and biocompatibility.⁷ However, despite being integrated into several biomedical devices,^{8,10–12} traditionally synthesized PU has experienced many challenges in biomedical applications due to toxic precursors and leaching of chemicals such as isocyanates, and other associated degradation products during their lifespan of operation.^{13–17} Conventionally, most PUs are produced by a reaction of polyols and isocyanates, which are commonly derived from a reaction of amine with highly toxic phosgene.^{15,18} The isocyanates have been reported as one of the primary causes of occupational asthma worldwide due to its volatility,^{13,14} and remained during the polymerization process and resulting PU materials.

Thus, there has been many attempts with increasing attention and societal pressure to find an alternative to produce non-isocyanate PUs, especially where toxicity to humans is a concern, such as in medical, foods, and children products.^{14,19,20} To avoid the issue of toxic precursors or unwanted leaching solutes associated with conventional polyurethane, the ring-opening conjugation reactions of five- and six-membered cyclic carbonates (MCC) with polyamines has been employed to create urethane bonds without the use of either phosgene or isocyanates.^{14,21–24} Recently, the syntheses of non-isocyanate PUs from five-MCC and amines have been reported as a sustainable route from different sources such as castor oil,²⁵ thioglycerol, fatty acids,²⁶ and hydroxyurethane methacrylate.²⁷ Meanwhile six-MCC showed much higher reactivity on the ring opening reaction with amine to form urethane bond than that of five-MCC.²⁸ Recently we have successfully demonstrated the production of various functional six-MCC from polyols and dimethylcarbonate,^{29,30} which is regarded as a green substance.³¹ Furthermore, by functionalizing the cyclic carbonate with an allyl group, UV light exposure can induce the terminal alkene to participate in a radical-mediated thiol–alkene (thiol–ene) reaction with a thiol group – this functionalized cyclic carbonate can then be used to impart different properties to the polymer. This thiol–ene chemistry is considered a click reaction: high efficiency, simple execution with limited side products, and high yields.³²

In recent years, thiol–ene chemistry has seen extended use in bulk materials, thin films, and nanofabrication applications.^{32,33} Thiol–ene systems of various compositions were printed *via* inkjet and cured with a xenon flash lamp system to produce mechanically- and chemically-stable dielectric films.³⁴ And, with increasing attention on the light-based 3D printing,^{35,36} thiol–ene chemistries have been used in printing,^{37–40} since the associated click reaction properties facilitate classical photopolymerization advantages of both spatial and temporal control,³² and enable the assembly of highly uniform crosslinked networks and polymer

functionalization^{41,42} for a variety of bioengineering applications.⁴³

Additional difficulties exist in acquiring commercially available photopolymerizable PU,³ which hamper its use in light-based 3D printing applications. While there are some commercially-available aliphatic polyurethane-diacrylate materials, such as an industrially-produced sealant known as Dymax® BR7432IG30, these have some shortcomings.⁴⁴

Here, we present a novel 3D-printable and tunable polymerization mechanism of non-isocyanate PUs (NIPU) networked with thiol crosslinkers *via* click chemistry. To improve the material's biocompatibility, we chose metabolic products of natural amino acids or derivatives as the polymer amine precursors. The chemical tunability and physical properties of this thiol–ene-NIPU are investigated in controlling rigidity, flexibility, and elasticity while also demonstrating non-toxicity, cytocompatibility, and compliant mechanism or device printing.

Results and discussion

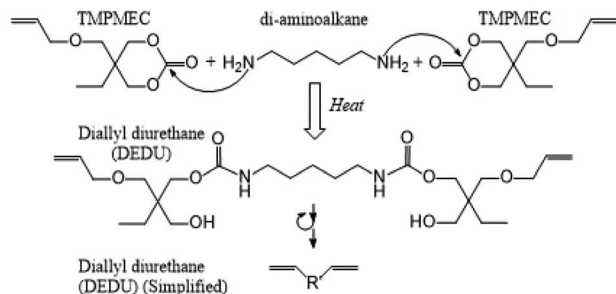
Functional diurethane prepolymer (DEDU) and non-isocyanate polyurethane (NIPU)

The ring opening conjugation of six-MCC with amines has attracted attention over the use of five-MCC chemistries in producing PUs without phosgene and isocyanate,^{14,21,23,45} due to the more reactive and thermodynamically-favorable reaction involved.¹⁴

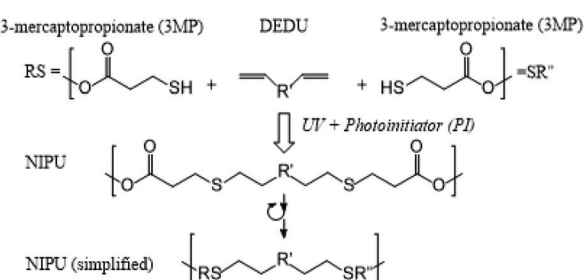
Fig. 1 shows an easily-tunable, “green” thiol–ene click-chemistry synthesis of PU using trimethylolpropane monoallyl ether cyclic carbonate (TMPMEC). The process consists of: (1) thermal formation of diurethane monomers from the ring opening reaction of the cyclic carbonate with amine, and (2) UV-induced free-radical end-linking polymerization of the allyl group with the thiol. Here, urethane molecules which are unique monomers and linkers, can be generated from a catalyst-free thermal reaction of TMPMEC with an amine group, and then the allyl functional monomers can be used to attach various thiols capable of imparting different properties to the polymer *via* thiol–ene polymerization.

Various biogenic polyamines such as putrescine, cadaverine, spermidine, and spermine, which are metabolites found in essential biosynthesis pathways, can be used to affect the degree of crosslinking,^{46,47} site-specific degradation, as well as the physical properties of the resulting polymers. These compounds are normally formed by the decarboxylation of amino acids as part of the normal metabolism of microorganisms, plants and animals. They are also present in a wide range of foods, including dairy products, and fermented foods, and can accumulate in high concentrations (*e.g.* >1000 mg per kilogram of cheese).^{14,43,45} In this work, cadaverine was used due to its structural simplicity and ubiquity as lysine's decarboxylation product in protein putrefaction. The two terminal primary amines of cadaverine produce a uniform length, cadaverine-

1) Thermal ring opening reaction of TMPMEC with multi-primary amine produces diallyl diurethane (di-alkene) (DEDU) co-monomer:



2) Diallyl diurethane (DEDU) co-polymerization reaction with chosen multi-thiol(s) via classical thiol-alkene reaction (4SH-DEDU-3SH example):



3) Examples of interchangeable macro-polymer branching via tetra-, tri-, and bis-thiol co-monomers used (mixtures also implemented):

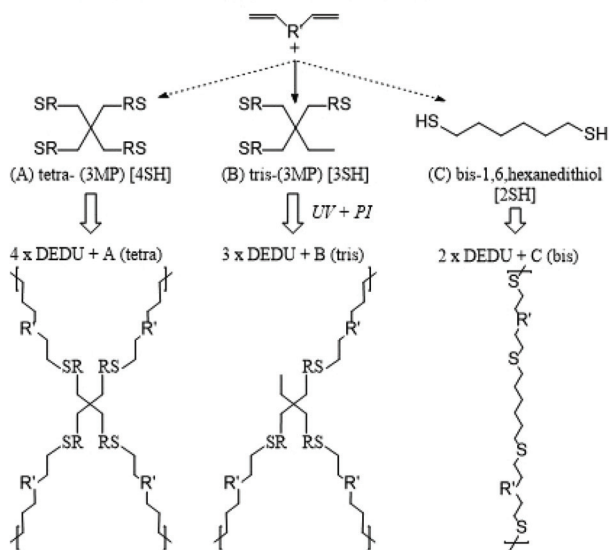


Fig. 1 Schematic of the NIPU polymerization system. Synthesis of diallyl urethane prepolymer from diamine and TMPMEC by heating, followed by UV-photoinitiated free radical thiol-ene polymerization with branched variable thiol crosslinkers, to create a 3D polymer network.

specific (di-ene) diurethane (csDEDU). This NIPU pre-polymer has a C5 alkane link between the urethanes and was referenced in step 1 of the process. The two urethane bonds are reaction products of two cyclic carbonates with one cadaverine *via* the ring opening reaction, without any use of phosgene, isocyanate or additional catalysts and qualify as a green

process. The resulting alkene-functionalized diurethane was incorporated with various ratios of branched multi-thiols (the second co-monomer used in end-linking and crosslinking), and then photopolymerized *via* UV light and a photoinitiator into thiol-ene crosslinked NIPU structures.

The reactants and products of the thermal ring opening and photopolymerization reactions were monitored to confirm transformation of functional groups using Fourier Transform Infrared Spectroscopy (FTIR) (Fig. 2). In the first step, the formation of diurethane from the ring opening of TMPMEC with cadaverine was monitored with a peak change of the carbonyl group at 1752 cm^{-1} , which diminishes (Fig. 2b). Meanwhile a new carbonyl peak appears at 1695 cm^{-1} resulting from transformation of cyclic carbonate to urethane, and coincides with the appearance of a broad hydroxyl peak ($3200\text{--}3600\text{ cm}^{-1}$) (Fig. 2c). During the second step, where functional diurethane monomers polymerize *via* UV-induced free radicals, a peak at 927 cm^{-1} correlating to the C-H of mono-substituted alkene in the allyl group disappeared as the new thiol-ene sulfide bond is formed (Fig. 2).

In the time course of UV reaction, a maximum FTIR peak of available alkene for thiol-ene polymerization at the initial time (0 minute, Fig. 2e) partially decreased at 2.5 minutes (Fig. 2f), and then completely decreased at 5 minutes (Fig. 2g), which was confirmed with no additional significant change in spectra after 10 minutes of exposure (Fig. 2h). These reactions were quantitatively carried out and completed without solvent or additional catalyst, and FTIR spectra were consistent for ring-opening and photopolymerizable mechanisms utilizing “green” click chemistries (full spectra in Fig. S1†).

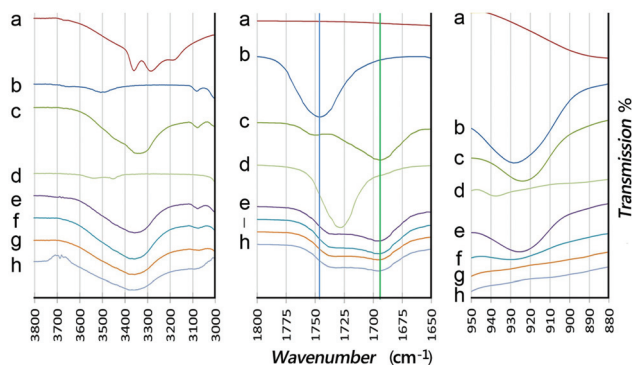


Fig. 2 FTIR spectra of molecular precursors and products. (a) Cadaverine. (b) TMPMEC [5-allyloxyethyl-5-ethyl-1,3-dioxane-2-one (trimethylolpropane allyl ether-cyclic carbonate)]. (c) Product of heating cadaverine in the presence of TMPMEC. Diallyl di-urethane (DEDU) product confirmed with replacement of cyclic-carbonate peaks with urethane ($\text{O}=\text{C}-\text{N}$) and hydroxyl ($-\text{OH}$) peaks. (d) Intermediate cross-linking thiol (3SH) = trimethylolpropane tris(3-mercaptopropionate). (e) Mixture of DEDU (c) and 3SH (d) exposed to 365 nm light for 0 min, (f) 2.5 min, (g) 5 min, and (h) 10 min. The peak at 927 cm^{-1} , indicative of the alkene, diminishes with time and shows no difference between (g) and (h). Samples run in triplicate ($n = 3$).

Tunable synthetic process and characteristics of NIPU

A polymer material with tunable physical properties is desirable for many practical applications, *e.g.* the biological relevance of polymer chain crosslinking usually imparts tension forces impacting cell differentiation, swelling, and cell integration.^{11,48–50} Both cyclic carbonate and thiol-ene chemistry afford more tunable and controllable approach to produce a wide spectrum of physical properties for the material structures. The reaction of key precursor molecules, TMPMEC, with a multi-primary amine molecule produced a highly uniform length isocyanate-free multi-allyl multi-urethane, as an alkene functionalized monomer and prepolymer. These uniform allyl urethane monomers, then polymerize with multi-thiols *via* the thiol-alkene click reaction producing a highly consistent length alternating thiol-[alkene-urethane-urethane-alkene]-thiol polymer. Additionally, the combination and mixture of types and ratios of the amines and thiols can be substituted to create numerous NIPU variants to meet various user demands and applications.

In this study, to better examine the tunability of NIPU material properties through crosslinking, only the relatively linear cadervine-specific diallyl diurethane (csDEDU) was used to limit any crosslinking to branched multi-thiols. The multi-thiols were chosen to introduce varied degrees of branching for the thiol-ene reaction with this specific csDEDU precursor. The tetra- and tri-thiols chosen reflect a conjugated deaminated cysteine, 3-mercaptopropionate structure for both tris and tetrakis variants. And 1,6-hexanedithiol was chosen as a simple, linear non-branching (low crosslinking) agent.

All NIPU material samples tested were specifically formulated to contain an equal molar ratio of alkene and thiol functional groups. Since csDEDU was the only alkene molecule for this study, the nomenclature adopted to convey contributing inter-nodal bond constituents of NIPU materials focuses on variation in thiols. NIPU materials are represented as a percent molar ratio of thiol functional group from each tetra-thiol_{4SH}, tris-thiol_{3SH}, and/or bis-thiol_{2SH} source. By adjusting the ratio combinations of thiols (Fig. S2†), the properties and networks of NIPU can be varied.

Dynamic and elastic deformation data

Dynamic mechanical analysis was used to compare compression properties of different NIPUs with the above self-imposed constraints (Fig. 3). Material compressibility is related to storage modulus E' data, which was used to evaluate elastic response (Fig. 3A). The highest storage moduli were found for both tetrakis-only and tris-only thiol-csDEDU mixtures. Interestingly, the three NIPU mixtures of tetrakis and tris 3-mercapto propionate co-monomers suggest that the lowest storage moduli was an equimolar ratio of tetrakis and tris thiol molecules. This behavior suggests greater packing or crosslinking density of the NIPU:50%_{4SH}-50%_{3SH} sample tested. 1,6-Hexanedithiol (2SH) was tested *via* other mixtures because csDEDU-2SH alone and csDEDU-3SH-2SH mixtures could not be directly tested at room temperature. 1,6-

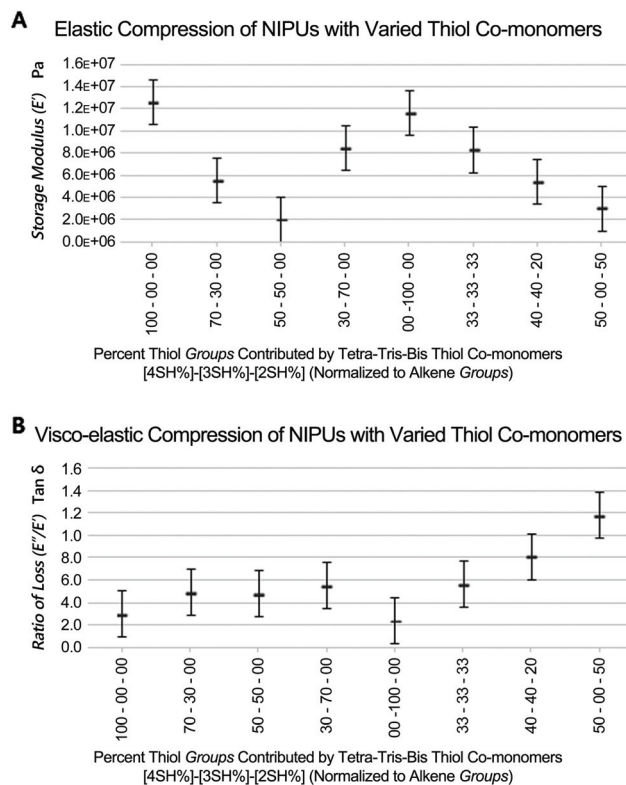


Fig. 3 Compression testing by dynamic mechanical analysis. Compositions of thiol crosslinker of NIPU evaluated based on mixtures measured for (a) storage modulus and (b) ratio of loss $\tan \delta$. (4SH) = pentaerythritol tetrakis(3-mercaptopropionate), (3SH) = trimethylolpropane tris(3-mercaptopropionate), and (2SH) = 1,6-hexanedithiol ($n = 3$).

Hexanedithiol had opposite effects on the lowest storage modulus NIPU:50%_{4SH}-50%_{3SH} and highest storage modulus NIPU:50%_{4SH}-50%_{3SH} base materials tested. In theory, NIPU:33%_{4SH}-33%_{3SH}-33%_{2SH} randomly incorporates 2SH into one-half of all inter-nodal 4SH-3SH molecular chains, increasing the maximum molecular length from 5.05 nm to 9.48 nm (+88%), and increasing the storage modulus ~ 4 times that of the non-2SH base material, NIPU:50%_{4SH}-50%_{3SH}. Sharing this trend NIPU:40%_{4SH}-40%_{3SH}-20%_{2SH} randomly incorporates 2SH into one-quarter of all inter-nodal 4SH-3SH molecular chains and has ~ 2.5 times the storage modulus of non-2SH base material, NIPU:50%_{4SH}-50%_{3SH}. This may be due to disruption of the quasi-crystalline^{33,51} structure or relaxation of the 4SH-3SH packing architecture.

In contradiction to the above trend, NIPU:50%_{4SH}-50%_{2SH} data matches intuition. Incorporation of 2SH into theoretically all inter-nodal 4SH-4SH molecular chains, produces a uniform quasi-crystalline structure of increased dimension and less crosslinking per volume, which decreases the storage modulus ~ 4 times. The 88%-dimensional increase coupled with the $\sim 4\times$ decreases from NIPU:50%_{4SH}-50%_{2SH} to NIPU:100%_{4SH} may suggest a square function similarity.

Three main categories arise from the $\tan \delta$ data values at room temperature (Fig. 3B). NIPU single species branching-

thiols (4SH or 3SH), mixtures of branching-thiols (4SH and 3SH), and linear thiol additions. Single species branching-thiols (4SH or 3SH) and mixtures (4SH and 3SH) do not show significant intra-group statistical differences and arguably, only show very slight inter-group statistical difference related to $\tan \delta$ "lossiness". While NIPU:50%_{4SH}-50%_{3SH} and NIPU:33%_{4SH}-33%_{3SH}-33%_{2SH} show no significant statistical difference, NIPU:40%_{4SH}-40%_{3SH}-20%_{2SH} shows increase in $\tan \delta$ (lossiness) despite a lower concentration and percentage of 2SH. Then, NIPU:50%_{4SH}-50%_{2SH} behaves as expected with a high "lossiness". This observation may potentially be related to bond uniformity in respect to the inability of creating a quasi-crystalline structure. The same inter-nodal bond lengths exist for all 4SH and 3SH polymerized chains.⁵² Conceptually 4SH only, and 3SH only material might form quasi-crystalline structures easier than 4SH/3SH mixtures due to lower species entropy and reflect this with the lowest $\tan \delta$ values. By extension equimolar 4SH/3SH material likely has more uniform inter-nodal structures, similar to NIPU:50%_{4SH}-50%_{3SH}. Although not perfect, if exactly half of the 4SH-3SH bonds are lengthened as in NIPU:33%_{4SH}-33%_{3SH}-33%_{2SH}, a square prism structure is a simple example of a quasi-crystalline organization that can accommodate a 1:1 ratio of 5.05 nm and 9.48 nm bonds. When this bond ratio length becomes 3:1 as in NIPU:40%_{4SH}-40%_{3SH}-20%_{2SH}, the lossiness increases, potentially due to structural artifacts arising from not being able to uniformly accommodate the quasi-crystalline organization. NIPU:50%_{4SH}-50%_{2SH}, a NIPU material with all bonds lengthened, fits Senyurts work of molecular chain length extension *via* their alkene co-monomer using a conventional thiol-ene non-PU polymer.⁵¹ This phenomenon may roughly correlate to a square function possibly relating to the tetra-thiol used, and is different from many telechelic acrylate polymers where increasing the monomer length does not influence the crosslinking frequency of the polyacrylate chain.

Young's modulus data

The stress-strain data details the forces required to deform or stretch a given material (Fig. S3 and S4†). Fig. 4 shows a general trend where increasing the concentration of tri-thiol crosslinker reduces the force required to elongate the polymer film.

As expected, when increasing the concentration of linear di-thiol, there is a stronger reduction in required elongation force. Materials with smaller Young's moduli tend to stretch farther than stiffer materials with the same force, however the majority of the materials encountered mechanical failure at the grip-material interface, thus their material failure data is inconclusive.

As seen in Fig. 4, the more rigid tetra-only thiol material NIPU:100%_{4SH} has the highest storage modulus and is resistant to stretching. Interestingly, the mixed tetra-/tri-thiol NIPU:50%_{4SH}-50%_{3SH} had a very low storage modulus, yet also showed high resistance to stretching; and the tri-only thiol NIPU:100%_{3SH} has a high storage modulus, yet has high stretchability. These seemingly mismatched set of character-

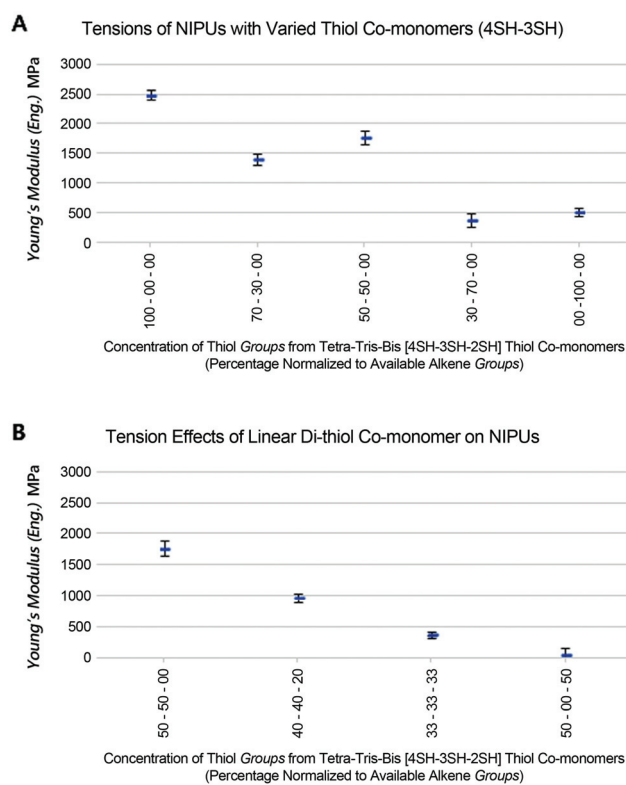


Fig. 4 Tension testing for engineering Young's modulus. Compositions of thiol crosslinker of NIPU evaluated based on mixtures used were measured for elastic deformation. (4SH) = pentaerythritol tetrakis (3-mercaptopropionate), (3SH) = trimethylolpropane tris(3-mercaptopropionate), and (2SH) = 1,6-hexanedithiol ($n = 5$).

istics demonstrate the potential tunability of thiol-ene network to create materials with varying rigidity, flexibility, and stretchability. The elastic-deformation modulus shows higher correlation to the type of bond branching rather than the expected crosslinking or storage modulus. An attenuated correlation also appears with materials likely to accommodate a consistent quasi-crystalline unit structure.

Swelling data and gel content

The internal polymer networks of NIPU polymers are difficult to examine once polymerized because the repeating units are large and flexible compared to crystals while still persisting as one large covalent macromolecule. Conventional methods for understanding bulk crystalline periodicity often rely on deconvolution of scattering spectra from highly-organized, immobile, periodic structures.

To circumvent these challenges, we used the amount of swelling and gel content to infer polymer network spacing and packing, assuming that the molecular chain tethers between junction nodes are approximately the same, and that the intermolecular solvation force between segments of the copolymer system is approximately uniform at equilibrium.^{33,51}

Because the NIPU swelling data found in Fig. 5 is dependent on the polymer network, there is less surprise that the

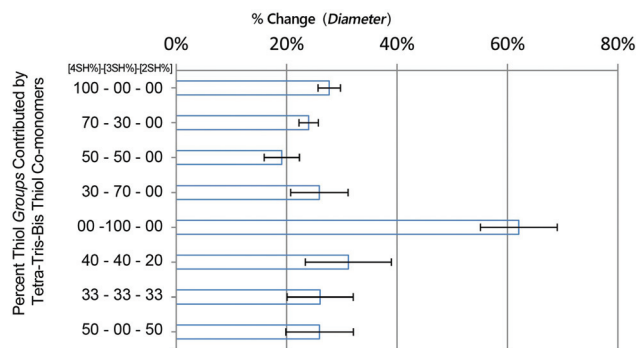


Fig. 5 Swelling analysis of NIPU material mixtures. Compositions of thiol crosslinker of NIPU evaluated based on mixtures used, swelling in chloroform based on disk diameter changes. (4SH) = pentaerythritol tetrakis (3-mercaptopropionate), (3SH) = trimethylolpropane tris(3-mercaptopropionate), and (2SH) = 1,6-hexanedithiol ($n = 3$).

swelling data roughly agrees with the storage modulus data, showing the highest values for tetra-thiol NIPU:100%_{4SH} and tri-thiol NIPU:100%_{3SH} and the lowest values for NIPU:50%_{4SH}-50%_{3SH} and other tetra/tri thiol blends. This swelling data reinforces the concept that a phenomenon with tetra/tri thiol blends is creating a denser and more restrictive network. The linear thiol materials' storage modulus data show slightly amplified ratios and larger error likely because the longer molecular chain lengths between branched cores permit more movement. The tri-thiol material swells to the highest degree, deviating from the tetra-thiol dominance in the storage modulus data. This “abnormal” swelling behavior indicates that the interval between network-anchored cross-linked bond lengths may be longer than expected for tri-thiol NIPU or related to possible chirality imposed by polymerization. For determining the degree of cross-linking, gel content was measured by extraction of soluble component from resulting NIPU, and showed over 90% resulted by highly cross-linking (Fig. S5†). Additionally, the storage moduli are high, suggesting an ordered packing regime such as laminar or sheet-like organization. While this was the only material where swelling tests were partially destructive due to rapid influx and outflux of the solvent, chloroform did not dissolve NIPU material even after 1+ week of submersion.

High solvent compatibility and resistance properties prohibited the measurement of molecular weight of the networked NIPU in solvent by gel permeation chromatography (GPC)-HPLC. Also, the thermal property of the new NIPU was evaluated by differential scanning calorimetry (DSC), and showed overall smooth energy flow during repeat heating and cooling processes which indicated the lack of a strong thermally induced internal crystallinity in the quasi-crystalline crosslinked NIPU for the thermal range. As NIPU intended “rubbery” phase is room temperature to 37 °C, a glass-transition is expected below this temperature range. The characteristics of a conventional glass-transition temperature (T_g) were observed at 2.33, -4.68 and -0.73 for NIPU:100%_{4SH}, NIPU:100%_{3SH}, and NIPU:50%_{4SH}-50%_{3SH} from the DSC data,

respectively (Fig. S6†). Furthermore, the data from DSC also indicate that these new NIPUs were thermally stable at temperatures as high as 250 °C in 2nd cycle. Thermogravimetric analysis (TGA) was performed to further investigate the thermal stability of the material, and similarly showed no thermal degradation of the material (Fig. S6†). From 20 to 250 °C, about 97% material weight maintained, and the small weight change started from the material being heated over 100 °C, which indicated that this insignificant weight change might be due to the evaporation of a small amount of residual water in the polymer material. The decomposition temperature was observed to be around 375 °C (50% weight loss) with no observable residue after 500 °C.

Green chemistry and biocompatibility data

Conventional PU production often involves toxic components such as isocyanates and phosgene. The process for NIPU production eliminates these contaminants, making it more suitable for biomedical usage.^{13,14} The ring-opening conjugation of cyclic carbonate with amines is an isocyanate-free process, and creates aliphatic PUs consisting of aliphatic urethanes, biogenic diamines, and thiols. Additionally, based on our understanding of NIPU synthesis and structure, NIPU without physicochemical or charge modification provides few motifs for cell adhesion. Since non-adhered cells tend to die, we grew high-density cell sheets on NIPU slabs to test for any potential cytocompatibility issues, relying on the aggregate cell-cell contact to correct for non-adhesion stimuli. Fig. 6A shows a NIPU slab tilted upside-down, the cell sheet has separated from the NIPU slab and is falling ‘forward’ from the viewer’s perspective toward the base of the cell culture plate. The living cell sheets were in direct contact with the NIPU slabs, but adhesion was sufficiently weak such that an air bubble was capable of displacing the cell sheet (Fig. S7†). The fluorescent images in Fig. 6A and B suggest minimal cell death (~3%) in response to prolonged NIPU contact as compared to the control (Fig. 6C, ~4%). In Fig. 6A and B, the murine C2C12 cells on a slab of NIPU:50%_{4SH}-50%_{3SH} proliferate under aggregated cell conditions despite lack of strong cellular adhesion and show little-to-no toxicity effects after 5 days of culture. Physisorbed fibronectin (Fig. 6B) did not substantially improve cell sheet adhesion to NIPU, however the cell sheets appear to show less clumping at the periphery. Cells from the surrounding polystyrene plate grew up to and around the NIPU slabs, as many cell sheets were found adhered to the culture plate. Based on the cell viability data, no acutely toxic effects were observed with the NIPU. Based on NIPU’s low-cell adhesion characteristic, this material may have application for structures with biofouling resistance or anti-coagulation coatings within the vasculature.

3D-Printed multi-mixture NIPU structures

3D projection printing was used to print different NIPU mixtures into 3D structures designed toward compliant mechanical devices to possess spatially-dependent storage moduli, Young’s moduli, flexibility, and stretchability. Fig. 7A shows

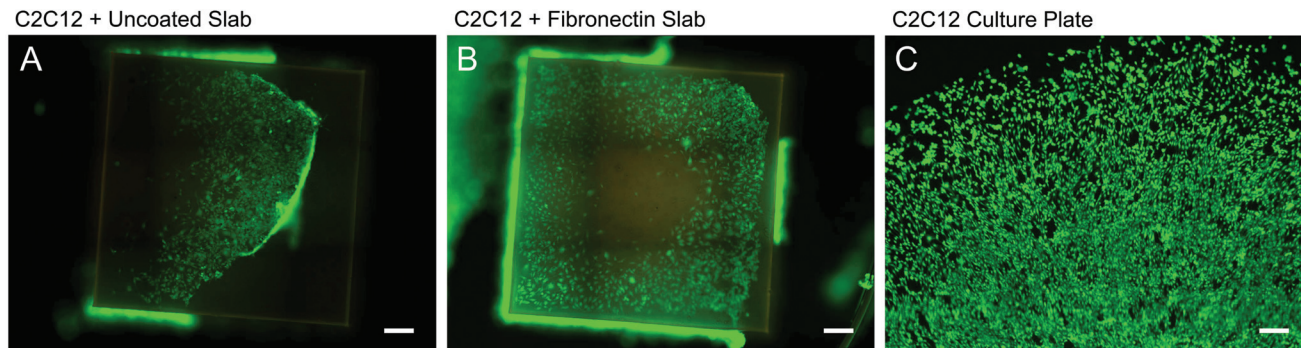


Fig. 6 Cell live/dead assay: Murine C3H C2C12 myoblasts grown on NIPU for 5 days. Green = Calcein AM, Red = Ethidium Bromide. (A, B) NIPU:50%_{4SH}–50%_{3SH} were tested. Uncoated (A) and physisorbed fibronectin (B) were examined to determine cell death. (C) Culture plate control. Structures were inverted for imaging (scale bar = 250 μm) (*n* = 9).

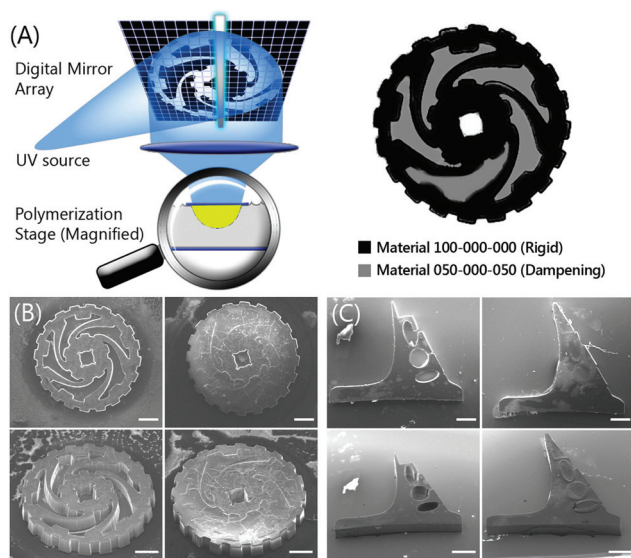


Fig. 7 3D printing of NIPU material: (A) schematic of the 3D projection printing setup with localization of printed materials. SEM images of printed NIPU structures; (B) a simple torque gear for dampening acceleration. (C) A pulsatile-flow cantilever valve. (B and C) Left images: More rigid material printed first. Right images: Compressible, damped, flexible, and elastic materials printed second (scale bar = 500 μm).

the 3D printing system schematic: UV-light illuminates a patterned digital mirror array, reflecting an optical pattern through focusing optics onto a moving stage containing NIPU prepolymer, thus photopolymerizing a 3D object. Fig. 7 shows various SEM images of stages in the 3D-printing primary and secondary NIPU materials of possible compliant mechanical devices.

Fig. 7B shows a directionally-biased semi-rigid gear with rotational dampening of acceleration. The design was inspired by wheels of NASA's Mars Pathfinder Rover that absorb tangential shock, however the same concept can be used to absorb or dampen rotational acceleration. The rationale is that miniaturized mechanical systems experience increased force-to-weight ratios – as artificial implants become more complex, they may

require dampened motion for mitigating of jerks or high rotational forces. In the first stage of printing, the 30 μm wide radial support dynamic struts, the axle contact, and gear teeth were printed with the more rigid tetra-thiol NIPU (NIPU:100%_{4SH}) (Fig. 7B). The unpolymerized NIPU:100%_{4SH} prepolymer was rinsed away, and followed by printing of the second prepolymer, NIPU:50%_{4SH}–0%_{3SH}–50%_{2SH}. The inner portions responsible for rotational dampening were printed with the more compressible and elastic mixture of tetra/di-thiol NIPU (NIPU:50%_{4SH}–0%_{3SH}–50%_{2SH}) (Fig. 7C).

Material NIPU:50%_{4SH}–0%_{3SH}–50%_{2SH} provides elastomeric dampening (lossiness), better distribution of force along the struts, and can prevent out-of-plane buckling. Thus, we demonstrate that modular formulations of NIPU can be combined synergistically for flexible applications.

Fig. 7C shows a cantilever of gradient thickness with flexion points that allow preferential bending after the application of varying forces. This design was envisioned as a cantilever valve for lab-on-a-chip (LOC) platforms examining variable pulsatile-flow in vascular indication models, and is designed to variably reduce the lag phase of fluid back flow during pulsatile flow. The two-step printing process used NIPU 100%_{4SH} and 50%_{4SH}–0%_{3SH}–50%_{2SH} for the rigid low compression backbone and stabilizing elastomeric regions, respectively. The varied regions of flexure reduce the valve closing time in situations where the flow rate may change, such as when experiencing system dilation, or the difference in cardiac output between infants and adults. NIPU's low cell adhesion properties may also provide an additional advantage in reducing biofouling and platelet adhesion.

Experimental

Materials and methods

Preparation of diallylated diurethane pre-polymer (csDEDU). 5-Allyloxyethyl-5-ethyl-1,3-dioxane-2-one (trimethylolpropane allyl ether-cyclocarbonate, TMPMEC) was prepared according to a previous report (NMR data in Fig. S8†).³⁰ Bio-based cadaverine (1,5-diaminopentane, >99%) was generously provided

by CJ Cheiljedang Corp. (South Korea). TMPMEC and cadaverine were mixed at a molar ratio of 2 : 1 in order to accommodate ring-opening conjugation with cadaverine's two available primary amines. This mixture of TMPMEC and cadaverine was initially vortexed vigorously for 1 min and then heated (68 °C for 15 min), during which it was also periodically vortexed. The resulting product, diallylated diurethane (csDEDU), was used with varying thiol compounds for photo-polymerization.

Preparation of photopolymerizable mixture. The branched thiol crosslinkers such as pentaerythritol tetrakis(3-mercaptopropionate) (>95%), trimethylolpropane tris(3-mercaptopropionate) (≥95.0%), and linear thiol 1,6-hexanedithiol (96%) were purchased from Sigma Aldrich. Darocur 1173® (2-hydroxy-2-methyl-1-phenyl-propan-1-one) purchased from Ciba Specialty Chemicals Inc. (Switzerland) was added as a liquid photoinitiator to the viscous prepolymer mixture. Various molar ratios of the multi-thiols were added to match the alkene bonds flanking the diallyl diurethane prepolymer. For instance of NIPU:100%_{4SH}, the mol ratio between diurethane (diene) and pentaerythritol tetrakis(3-mercaptopropionate) (4 thiols, 4SH) was 1 : 0.5. Meanwhile NIPU:50%_{4SH}-0%_{3SH}-50%_{2SH} were prepared from 1 : 0.25 : 0.5 ratio of diurethane (diene), pentaerythritol tetrakis(3-mercaptopropionate) (4 thiols, 4SH) and 1,6-hexanedithiol (2 thiols, 2SH), thus two thiol compounds contributed equally.

Each mixture was heated to 78 °C for 5 min. After heating, Darocur 1173® was added to each mixture at (2% v/v) and periodically vortexed for an additional 5 min at 78 °C.

FTIR analysis. FTIR spectra were acquired from a PerkinElmer® Spectrum Two infrared spectrometer equipped with a UATR (universal attenuated total reflectance crystal) 2 module. Liquids were placed directly onto and completely covering the crystal sample window. Solid materials of various compositions used were polymerized into 1 mm slabs and then cut into disks with a 6 mm biopsy punch. Spectra from the material-face distal to the UV light source are reported. Spectra from material-faces were shown to be consistent at the 927 cm⁻¹ peak indicating the alkene-associated carbon-hydrogen bond. This alkene-associated carbon-hydrogen bond is affected by alkene-thiol conjugation and indicative of polymerization of the material.

Dynamic compression storage modulus. A PerkinElmer® Dynamic Mechanical Analyzer (DMA 8000) was used to obtain storage modulus and “lossiness ratio” (tan δ) compression data. Frequency scans were run from 0.1 to 3.0 Hz at 5% displacement on 1 mm thick, 6 mm wide disks of the various materials used that had been polymerized *via* 365 nm UV light for 5 min. The frequency curve was checked for continuity and the 1 Hz point was reported in order to compare the various mixtures.

Tensile: Young's modulus. NIPU films were polymerized *via* 2 min of 365 nm UV light into films of various lengths (0.32 mm thick and 2.2–2.6 mm wide), and then examined. A PerkinElmer® TMA 7 running Pyris® was used to acquire tension data. Force-displacement curves were translated into stress-strain curves with the caliper measurements of the

material setup conformation. The moduli of various materials were acquired as the initial slope of the “linear” elastic-deformation region of the stress-strain curve meeting ($R^2 > 0.9999$) (Fig. S4†).

Analysis of swelling and gel content. The NIPU mixtures used were photopolymerized *via* 5 min of 365 nm UV light into slabs of 1 mm thick, and then cut into 6 mm wide disks with biopsy punches. The disks were submerged in chloroform for 5 min (saturation normally occurs at ~2 min), removed from chloroform, and quickly measured with calipers to determine swelling characteristics. The gel content (insoluble content) was determined by extraction of soluble part from the sample in boiling toluene for 24 h.^{53,54} The treated solid samples were dried in an oven at 50 °C till constant weight. It was calculated from the ratio of the residual mass (W_1) to the initial mass (W_0) by the following equation: Gel content (%) = $W_1/W_0 \times 100$.

Thermal analysis

Differential scanning calorimetry (DSC) was carried out using a DSC Q1000 (TA Instrument) over a temperature range of -80–250 °C with a 10 °C min⁻¹ heating rate under nitrogen. DSC was performed by 2 cycles of heating and cooling. DSC was performed by 2 cyclings of heating and cooling. Thermogravimetric analysis (TGA) curves were obtained by TGA Q5000 (TA Instrument) with a heating rate of 10 °C min⁻¹ under nitrogen with a flow rate of 35 cm³ min⁻¹.

3D printing by projection photopolymerization

We carried out 3D printing of NIPU using the printer setup as previously developed in our lab.^{36,55} 2D bitmap computer model slices are serially-uploaded to a digital micro-mirror device (DMD) chipset (1920 × 1080, Discover 4000 digital light processing (DLP) chip, Texas Instruments) that display dynamic patterns based on z-dimension height. The 2D bitmap slice information encodes a spatial pattern *via* tilting of individually-addressable micromirrors on the DMD chip. The tilted micromirrors reflect the UV source's light (Omnicure® S2000) through lenses to a focal point on a controllable sample stage. Stage movement was managed with a stage controller (Newport, CA) to change the optical focal plane height within the sample. A 320 nm–500 nm filtered light spectrum is produced by Omnicure® halogen bulbs. Synchronization of spatial patterns, light exposure, and z-focus with the sample chamber was controlled by a desktop computer. NIPU liquid pre-polymer mixture was diluted 20% v/v with 99.9% ethanol to minimize perturbing forces during rinsing of unpolymerized pre-polymer. The NIPU (80%)/ethanol (20%) mixture was physically confined with a transparent glass coverslip coated with Krytox® oil to prevent non-specific adhesion, and PDMS sheets were used in 3D printing. NIPU material was polymerized with 365 nm UV light for 45 to 90 seconds. Various NIPU structures were constructed by sequential photopolymerization of different NIPU/ethanol pre-polymer mixtures, thus creating single structures with multiple material properties. The printed 3D structures using NIPU were rinsed with ethanol (99%), heated at 68 °C for 15 min, and then

transferred to a room temperature vacuum chamber for 24 hours. The NIPU structures were sputter coated with carbon and imaged *via* a field emission environmental microscope (FEI XL30 ESEM FEG). Images were acquired in electron scattering mode at 10 kV.

Biocompatibility of NIPU slab construction for cells and fibronectin physisorption. NIPU square slabs were photopolymerized for 60 seconds at 6 W cm^{-2} . They were then rinsed with ethanol, heated at $68 \text{ }^\circ\text{C}$ for 10 min, and placed in a room temperature vacuum chamber for 24 h. Half of these materials were removed for fibronectin physisorbed coating at a concentration of 1 mg mL^{-1} dispensed directly onto the sample surface, and then allowed to incubate for 24 h at $4 \text{ }^\circ\text{C}$ protected from light. Afterwards, they were transferred to a vacuum chamber at room temperature for an additional 48 h. The dry samples were exposed to germicidal UV light for ~ 30 min prior to use.

Murine myoblast (C2C12) cells from ATCC® were cultured based on ATCC guidelines. The growth medium consisted of high glucose DMEM (Gibco), (inactivated) fetal bovine serum (10% v/v) (Hyclone), and L-glutamine (1%) (Gibco). Penicillin/streptomycin (50 units per mL) (Gibco) was added to the culture medium used during material-cell incubation. Cells were incubated at $37 \text{ }^\circ\text{C}$ with a gas mixture of 5% CO_2 and were sub-cultured prior to confluence. Cells were used at passage 6 and seeded on both fibronectin-coated (physisorbed) and bare NIPU:50%_{4SH}-50%_{3SH} slabs. The NIPU:50%_{4SH}-50%_{3SH} slabs were seeded with a $10 \mu\text{L}$ drop containing 2.0×10^4 cells and then incubated for 20 min at $37 \text{ }^\circ\text{C}$, after which the sample wells were carefully flooded to fully submerge the slab in complete growth medium.

C2C12 cells were seeded on polymerized NIPU:50%_{4SH}-50%_{3SH} with and without fibronectin coating. A LIVE/DEAD® Viability/Cytotoxicity kit for mammalian cells from Thermo Fisher Scientific was used to assess cytotoxicity on culture days 3 and 5. The culture media of each sample was removed and rinsed 3 times with an equivalent volume of DPBS (pH 7.4) before adding $150 \mu\text{L}$ of a cell-staining solution containing $2 \mu\text{M}$ calcein AM and $4 \mu\text{M}$ ethidium bromide in DPBS (Gibco) per Thermo Fisher guidelines. The cells were covered from light and then incubated with the staining solution at room temperature for 30 min. After incubation, the cell staining solution was removed, rinsed with 3 equivalent volumes of DPBS (pH 7.4), and then imaged using a Leica DMI 6000B microscope at the $10\times$ objective, with tiling functionality. Bright field and fluorescent images were taken, and a longer exposure time for the ethidium dye was used to enhance imaging of any dead cells against the fluorescent background.

Conclusions

We demonstrated a novel process to produce non-isocyanate PUs in a two-step synthesis consisting of a thermal ring opening reaction of functional cyclic carbonates with a diamine, and UV polymerization of the resulting diallyl diur-

ethane prepolymer with thiol cross-linkers by click chemistry. Physical properties of NIPUs from different combinations of linear and branched thiols were characterized, and shown to be tuneable, cytocompatible, and printable *via* light-based 3D printing, thus demonstrating the capability to spatially pattern different materials into novel, biocompatible mechanically-compliant structures. The tunability and characteristics of printable NIPU materials can be enhanced by using other types of biogenic polyamines such as putrescine (C4-diamine), spermidine (tri-amine) and spermine (tetra-amine) instead of cadaverine (C5-diamine), to regulate the chain length and degree of cross-linking. Furthermore, the green chemistry involved in NIPU synthesis eliminates hazardous leaching solutes such as phosgene, aromatic amines, and isocyanates, thus opening new pathways for PU cytocompatibility and its broader use in biomedical engineering.

Conflicts of interest

There are no conflicts to declare.

Acknowledgements

The project described was supported in part by the National Institutes of Health (R21AR074763, R01EB021857), and National Science Foundation (1644967 and 1907434). The work was also supported by the Swedish Research Council Formas for Environment, Agricultural Sciences and Spatial Planning (942-2016-63) to S.-H. P. Additionally, we thank the UCSD Materials Research Center for use of SEM, DMA, TMA and FTIR equipment, along with valuable assistance from Prof. Darren Lapomi, Sabine Faulhaber, and Wayne Neilson.

Notes and references

- 1 F.-M. Chen and X. Liu, *Prog. Polym. Sci.*, 2016, **53**, 86–168.
- 2 F. P. W. Melchels, J. Feijen and D. W. Grijpma, *Biomaterials*, 2010, **31**, 6121–6130.
- 3 I. H. L. Pereira, E. Ayres, P. S. Patricio, A. M. Goes, V. S. Gomide, E. P. Junior and R. L. Orefice, *Acta Biomater.*, 2010, **6**, 3056–3066.
- 4 T. Billiet, M. Vandenhaute, J. Schelfhout, S. Van Vlierberghe and P. Dubruel, *Biomaterials*, 2012, **33**, 6020–6041.
- 5 C. Cha, P. Soman, W. Zhu, M. Nikkhah, G. Camci-Unal, S. Chen and A. Khademhosseini, *Biomater. Sci.*, 2014, **2**, 703–709.
- 6 N. Chirani, L. H. Yahia, L. Gritsch, F. Leonardo, S. Chirani and S. Fare, *J. Biomed. Sci.*, 2015, **4**(2), 13.
- 7 J. Kucinska-Lipka, I. Gubanska, H. Janik and M. Sienkiewicz, *Mater. Sci. Eng., C*, 2015, **46**, 166–176.
- 8 P. Singhal, W. Small, E. Cosgriff-Hernandez, D. J. Maitland and T. S. Wilson, *Acta Biomater.*, 2014, **10**, 67–76.

- 9 R. S. Bezwada, *U.S. Pat. Appl. Publ.*, 2006, 38pp., Cont.-in-part of U.S. Ser. No. 233,876.
- 10 A. T. Stevenson, L. M. Reese, T. K. Hill, J. McGuire, A. M. Mohs, R. Shekhar, L. R. Bickford and A. R. Whittington, *Biomaterials*, 2015, **54**, 168–176.
- 11 Q. Chen, S. Liang and G. A. Thouas, *Prog. Polym. Sci.*, 2013, **38**, 584–671.
- 12 E. Richard, B. Mead, E. Zlotnikov, H. Park, N. J. Us, D. Haders and S. Nj, DOI: 10.1145/634067.634234.
- 13 J. E. Lockey, C. A. Redlich, R. Streicher, A. Pfahles-Hutchens, P. B. J. Hakkinen, G. L. Ellison, P. Harber, M. Utell, J. Holland, A. Comai and M. White, *J. Occup. Environ. Med.*, 2015, **57**, 44–51.
- 14 S.-H. Pyo, P. Persson, M. A. Mollaahmad, K. Sørensen, S. Lundmark and R. Hatti-Kaul, *Pure Appl. Chem.*, 2011, **84**, 637–661.
- 15 D. Heederik, P. K. Henneberger and C. A. Redlich, *Eur. Respir. Rev.*, 2012, **21**, 112–124.
- 16 P. Vermette, *Biomedical applications of polyurethanes*, Landes Bioscience, 2001.
- 17 H. Panwar, G. V. Raghuram, D. Jain, A. K. Ahirwar, S. Khan, S. K. Jain, N. Pathak, S. Banerjee, K. K. Maudar and P. K. Mishra, *Environ. Toxicol.*, 2014, **29**, 284–297.
- 18 P. Vermette, H. Griesser, G. Laroche and R. Guidoin, *Biomedical applications of polyurethanes*, 2001.
- 19 R. E. Chapin, J. Adams, K. Boekelheide, L. E. Gray, S. W. Hayward, P. S. J. Lees, B. S. McIntyre, K. M. Portier, T. M. Schnorr, S. G. Selevan, J. G. Vandenberg and S. R. Woskie, *Birth Defects Res., Part B*, 2008, **83**, 157–395.
- 20 O. Kreye, H. Mutlu and M. A. R. Meier, *Green Chem.*, 2013, **15**, 1431.
- 21 V. M. Lombardo, E. A. Dhulst, E. K. Leitsch, N. Wilmot, W. H. Heath, A. P. Gies, M. D. Miller, J. M. Torkelson and K. A. Scheidt, *Eur. J. Org. Chem.*, 2015, **2015**, 2791–2795.
- 22 X. Sheng, G. Ren, Y. Qin, X. Chen, X. Wang and F. Wang, *Green Chem.*, 2015, **17**, 373–379.
- 23 M. Kathalewar, A. Sabnis and D. D'Mello, *Eur. Polym. J.*, 2014, **57**, 99–108.
- 24 A. Cornille, R. Auvergne, O. Figovsky, B. Boutevin and S. Caillol, *Eur. Polym. J.*, 2017, **87**, 535–552.
- 25 L. Ruiz, A. Aghmiz, A. M. Masdeu-Bultó, G. Lligadas, J. C. Ronda, M. Galià and V. Cádiz, *Polymer*, 2017, **124**, 226–234.
- 26 O. Lamarzelle, G. Hibert, S. Lecommandoux, E. Grau and H. Cramail, *Polym. Chem.*, 2017, **8**, 3438–3447.
- 27 M. Decostanzi, C. Bonneaud and S. Caillol, *J. Polym. Sci., Part A: Polym. Chem.*, 2019, **57**, 1224–1232.
- 28 H. Tomita, F. Sanda and T. Endo, *J. Polym. Sci., Part A: Polym. Chem.*, 2001, **39**, 162–168.
- 29 S. H. Pyo, P. Persson, S. Lundmark and R. Hatti-Kaul, *Green Chem.*, 2011, **13**, 976–982.
- 30 S. H. Pyo and R. Hatti-Kaul, *Adv. Synth. Catal.*, 2016, **358**, 834–839.
- 31 S. H. Pyo, J. H. Park, T. S. Chang and R. Hatti-Kaul, *Curr. Opin. Green Sustain. Chem.*, 2017, **5**, 61–66.
- 32 C. E. Hoyle and C. N. Bowman, *Angew. Chem., Int. Ed.*, 2010, **49**, 1540–1573.
- 33 M. J. Kade, D. J. Burke and C. J. Hawker, *J. Polym. Sci., Part A: Polym. Chem.*, 2010, **48**, 743–750.
- 34 B. C. Riggs, R. Elupula, S. M. Grayson and D. B. Chrisey, *J. Mater. Chem. A*, 2014, **2**, 17380–17386.
- 35 K. C. Hribar, P. Soman, J. Warner, P. Chung and S. Chen, *Lab Chip*, 2014, **14**, 268–275.
- 36 P. Soman, P. H. Chung, A. P. Zhang and S. Chen, *Biotechnol. Bioeng.*, 2013, **110**, 3038–3047.
- 37 A. S. Quick, J. Fischer, B. Richter, T. Pauloehr, V. Trouillet, M. Wegener and C. Barner-Kowollik, *Macromol. Rapid Commun.*, 2013, **34**, 335–340.
- 38 H. Leonards, S. Engelhardt, A. Hoffmann, L. Pongratz, S. Schriever, J. Bläsius, M. M. Wehner and A. Gillner, *Proc. SPIE*, 2015, 9353, 93530F (International Society for Optics and Photonics).
- 39 S. C. Ligon, R. Liska, J. Stampfl, M. Gurr and R. Mülhaupt, *Chem. Rev.*, 2017, **117**, 10212–10290.
- 40 L. Chen, Q. Wu, G. Wei, R. Liu and Z. Li, *J. Mater. Chem. C*, 2018, **6**, 11561–11568.
- 41 A. Dondoni and A. Marra, *Chem. Soc. Rev.*, 2012, **41**, 573.
- 42 P. Thirumurugan, D. Matosiuk and K. Jozwiak, *Chem. Rev.*, 2013, **113**, 4905–4979.
- 43 H. Shih and C. C. Lin, *Biomacromolecules*, 2012, **13**, 2003–2012.
- 44 C. N. 5888-33-5 Sigma-Aldrich, Isobornyl acrylate | Sigma-Aldrich.
- 45 K. D. Belfield, S. Yao, A. R. Morales, J. M. Hales, D. J. Hagan, E. W. Van Stryland, V. M. Chapela and J. Percino, *Polym. Adv. Technol.*, 2005, **16**, 150–155.
- 46 B. Ochiai, J. I. Nakayama, M. Mashiko, Y. Kaneko, T. Nagasawa and T. Endo, *J. Polym. Sci., Part A: Polym. Chem.*, 2005, **43**, 5899–5905.
- 47 M. Bähr and R. Mülhaupt, *Green Chem.*, 2012, **14**, 483.
- 48 J. W. Nichol, S. T. Koshy, H. Bae, C. M. Hwang, S. Yamanlar and A. Khademhosseini, *Biomaterials*, 2010, **31**, 5536–5544.
- 49 K. Yue, G. Trujillo-de Santiago, M. M. Alvarez, A. Tamayol, N. Annabi and A. Khademhosseini, *Biomaterials*, 2015, **73**, 254–271.
- 50 G. Kumar, M. S. Waters, T. M. Farooque, M. F. Young and C. G. Simon, *Biomaterials*, 2012, **33**, 4022–4030.
- 51 A. F. Senyurt, H. Wei, B. Phillips, M. Cole, S. Nazarenko, C. E. Hoyle, S. G. Piland and T. E. Gould, *Macromolecules*, 2006, **39**, 6315–6317.
- 52 M. J. Kade, D. J. Burke and C. J. Hawker, *J. Polym. Sci., Part A: Polym. Chem.*, 2010, **48**, 743–750.
- 53 S. A. Riyajan and W. Sukhlaaied, *Mater. Sci. Eng., C*, 2013, **33**, 1041–1047.
- 54 M. Jaunich, M. Böhning, U. Braun, G. Teteris and W. Stark, *Polym. Test.*, 2016, **52**, 133–140.
- 55 C. A. P. Zhang, X. Qu, P. Soman, K. C. Hribar, J. W. Lee, S. Chen and S. He, *Adv. Mater.*, 2012, 4266–4270.